

# A Domain Decomposition Method for Kinetic-Hydrodynamic Multiscale Problems in Gas Dynamics and Device Simulations Using the Discontinuous Galerkin Methods

Shanqin Chen<sup>1</sup>, Weinan E<sup>2</sup>, Yunxian Liu<sup>3</sup> and Chi-Wang Shu<sup>4</sup>

## Abstract

In this paper we develop a domain decomposition method (DDM), based on the discontinuous Galerkin (DG) and the local discontinuous Galerkin (LDG) methods, for solving multiscale problems involving macro sub-domains, where a macro model is valid, and micro sub-domains, where the macro model is not valid and a more costly micro model must be used. We take two examples, one from compressible gas dynamics where the micro sub-domains are around shocks, contacts and corners of rarefaction fans, and another one from semiconductor device simulations where the micro sub-domains are around the jumps in the doping profile. The macro model is taken as the Euler equations for the gas dynamics problem and as a hydrodynamic model and a high field model for the semiconductor device problem. The micro model for both problems is taken as a kinetic Bhatnagar-Gross-Krook (BGK) equation. We pay special attention to the effective coupling between the macro sub-domains and the micro sub-domains, in which we utilize the advantage of the discontinuous Galerkin method in its compactness of the computational stencil. Numerical results demonstrate the effectiveness of our DDM-DG method in solving such multi-scale problems.

**Key Words:** domain decomposition method, discontinuous Galerkin method, gas dynamics, semi-conductor device simulation, hydrodynamics model, high-field model

---

<sup>1</sup>Department of Mathematics, University of California at Irvine, Irvine, CA 92697. E-mail: shanqin@math.uci.edu

<sup>2</sup>Department of Mathematics, Princeton University, Princeton, NJ 08544-1000. E-mail: weinan@math.princeton.edu. The research of this author is supported in part by ONR grant N00014-01-1-0674 and by NSFC grant 10128102.

<sup>3</sup>School of Mathematics and System Sciences, Shandong University, Jinan, Shandong 250100, China. E-mail: yxliu@sdu.edu.cn. The research of this author is supported in part by NNSF of China.

<sup>4</sup>Division of Applied Mathematics, Brown University, Providence, RI 02912. E-mail: shu@dam.brown.edu. The research of this author is supported in part by ARO grant W911NF-04-1-0291, NSF grant DMS-0510345 and AFOSR grant FA9550-05-1-0123.

# 1 Introduction

In this paper we are interested in numerical simulations of a type of multiscale problems that contain isolated defects or singularities such as cracks, dislocations, shocks and contact lines. A common feature of such multiscale problems is that the computational domain can be decomposed to two types of sub-domains. The first type contains macro sub-domains, where a computationally inexpensive macro model is valid. The second type contains micro sub-domains, where the simple macro model is not valid and a more costly micro model must be used. In many such problems, the size of the micro sub-domains is relatively small. Typically, such multiscale problems are solved by a domain decomposition method (DDM), see for example [1, 2, 3, 4, 5, 7, 17, 18, 19, 20, 23, 24, 26, 27, 28, 29]. The success of DDM depends on the numerical solvers used in the macro and micro sub-domains, and more importantly on the interfacing between these two types of sub-domains.

We will apply the discontinuous Galerkin (DG) and the local discontinuous Galerkin (LDG) methods for both the macro and the micro sub-domains. The DG method is a finite element method which uses discontinuous piecewise polynomials as basis functions and relies on an adequate choice of numerical fluxes, which handle effectively the interactions across element boundaries, to achieve stable and accurate solutions for nonlinear hyperbolic conservation laws. The particular version of the DG method that we use in this paper is the Runge-Kutta discontinuous Galerkin (RKDG) method, see, e.g. [12, 11, 10, 13, 15]. For nonlinear convection diffusion equations and other partial differential equations (PDEs) involving higher order spatial derivatives, we use the LDG method [14, 33]. For more details of the DG and LDG methods, see for example the review paper [15]. The DG methodology allows easy  $h$ - $p$  adaptivity and efficient parallel implementation. However, the main advantage of the DG method in our DDM context is the fact that the DG methods have very compact stencils: the evolution of the numerical solution in a given cell depends only on the information of immediate neighbors through the numerical fluxes at the element boundary, regardless of the order of accuracy. This advantage helps to simplify the interfacing

treatment between the macro and the micro sub-domains, for we would only need to define adequately the numerical fluxes at such interfaces to transfer information between the two sub-domains and do not need to define any ghost point values in the neighboring sub-domain.

As prototype examples to demonstrate the methodology, we consider only one dimensional problems in this paper and leave multi-dimensional study to future work. We concentrate our attention on two examples, one from compressible gas dynamics where the micro sub-domains are around shocks, contacts and corners of rarefaction fans, and another one from semiconductor device simulations where the micro sub-domains are around the jumps in the doping profile. In this paper we do not explore the strategy of effectively identifying the macro and micro sub-domains and simply define them *a priori* based on the application problems.

The macro models are taken as the Euler equations for the gas dynamics problem and as a hydrodynamic (HD) model and a high field (HF) model for the semiconductor device problem. The micro model for both problems is taken as a kinetic BGK equation. Since we emphasize the DDM methodology rather than the physics, we choose the simple BGK model rather than models with more complex collisions to avoid unnecessary technical difficulty for numerical simulation. However our methodology can be easily applied to the situation where the micro model is the Boltzmann equation with more complex collision terms (e.g. [9]) or other equations. Physically, the micro scale kinetic equation provides more information about the flow and has larger applicability than the macroscopic counterpart. Unfortunately, when the mean free path becomes small, the numerical solution of these equations becomes very costly, as the grid size used in the discretization must be smaller than the mean free path. Also, kinetic problems have twice the dimension as the macro problems and are costly to simulate in any case. The main idea of DDM is to solve the relatively inexpensive macroscopic model in most part of the computational domain, and only solve the micro problems in the sub-domain where the macroscopic model is not valid.

A major emphasis of this paper is on the effective coupling between the macro and micro

sub-domains, in which we utilize the advantage of the discontinuous Galerkin method in its compactness of the computational stencil. It is usually easier to transfer information from a micro sub-domain to a macro sub-domain, where one only needs to take moments of the distribution function from the micro sub-domain solution to provide the necessary boundary data for the macro sub-domain. To transfer information from a macro sub-domain to a micro sub-domain is more subtle, as one would need to choose an ansatz of the distribution function in order to use the limited information from the solution in the macro sub-domain to determine the necessary boundary data for the micro sub-domain. In most of the DDM calculations, this ansatz is taken as a Maxwellian or another known equilibrium distribution function, often obtained analytically from asymptotic analysis. Such an approach works well for our gas dynamics test problems as the distribution function near the interfaces of the macro and micro sub-domains is close to the equilibrium Maxwellian. However, this approach does not work well for our semi-conductor device simulation example, see [5, 7]. The difficulty comes from the fact that the distribution function near the macro to micro interface in the low doping region is still significantly different from the Maxwellian or the high field ansatz [8] determined from an asymptotic analysis. We propose an approach where the ansatz of the distribution function at the interface is determined by the numerical solution in the micro sub-domain at the interface, with its height adjusted and its velocity shifted and scaled by the macro information provided from the macro sub-domain. This approach works very well in our semi-conductor device simulation for a silicon diode.

We would like to remark that the “Type A” problems in the heterogeneous multi-scale method (HMM) framework [16] have many common features with DDM. The main difference between DDM style methods and HMM style methods is that HMM style methods also try to address different time scales between the micro and macro sub-domains. In this paper we have not addressed these time scale variation issues, as the examples and resolutions we have chosen yield comparable time evolution scales between the micro and macro sub-domains.

The kinetic equation is solved directly in this paper. In many cases, this may not be

the preferred approach in regard to computational efficiency. Our approach, especially the coupling technique between the micro and macro sub-domains, applies in principle also to the situation when the kinetic equation is replaced by direct simulation Monte Carlo (DSMC). This is however not pursued in this paper.

The organization of the paper is as follows. In section 2 we describe the DDM-DG method for the one-dimensional gas dynamics problem, namely coupled Boltzmann and Euler equations, and provide numerical examples. In section 3 the DDM-DG method for the one-dimensional diode simulation problem in semiconductor devices is given, with numerical examples. Concluding remarks are given in section 4.

## 2 Continuum gas dynamic problems

There are two ways to describe a flow motion. The first one is based on macroscopic quantities, such as mass, momentum and energy densities, as well as the physical law governing these quantities, such as Euler, Navier-Stokes or higher order approximate equations supplied by the equation of state. The other description comes from microscopic considerations, i.e. the gas kinetic theory. In this paper, we will only treat one-dimensional flow as prototype examples and will only describe briefly the gas kinetic theory. For more details, see for example [32].

The fundamental quantity in the gas kinetic description is the particle distribution function  $f(x, \xi, t, \varepsilon)$  which gives the density of molecules in the two-dimensional physical-phase space  $(x, \xi)$ , where  $(x, t)$  is the location of any point in space and time and  $\xi$  is the particle velocity. The additional variables  $\varepsilon = (\varepsilon_1, \dots, \varepsilon_K)$  are the components of the internal particle velocity in  $K$  dimensions. They appear when there is internal motion happening in molecules, such as rotation and vibration. The dimension of the internal variables is related to the gas constant  $\gamma$  in the following way

$$K = \frac{3 - \gamma}{\gamma - 1}.$$

The evolution equation for the gas distribution function  $f$  is the Boltzmann equation

$$f_t + \xi f_x + a f_\xi = Q(f, f)$$

where  $a$  is the external force term acting on the particle, and  $Q(f, f)$  is the collision operator. The corresponding relationship between the macroscopic quantities and the microscopic distribution function  $f$  is

$$\begin{pmatrix} \rho \\ m \\ E \end{pmatrix} = \int_{\mathbb{R}} f(x, \xi, t, \varepsilon) \begin{pmatrix} 1 \\ \xi \\ \frac{1}{2}(\xi^2 + \varepsilon_1^2 + \dots + \varepsilon_K^2) \end{pmatrix} d\xi d\varepsilon_1 \dots d\varepsilon_K,$$

where  $\rho$  is the density,  $m = \rho v$  the momentum, and  $E$  the energy, satisfying the equation of state

$$E = \frac{p}{\gamma - 1} + \frac{1}{2} \rho v^2,$$

where  $v$  is the velocity of the hydrodynamic flow, and  $p$  is the pressure of the gas. Due to the unique format of the equilibrium distribution function  $M$  in classical statistical physics, at each point in space and time, there is a one to one correspondence between  $M$  and the macroscopic densities, e.g. mass, momentum and energy. This equilibrium distribution is the so-called Maxwellian,

$$M(x, \xi, t, \varepsilon) = \frac{\rho(x, t)}{(2\pi\theta(x, t))^{\frac{K+1}{2}}} \exp\left(-\frac{(\xi - v(x, t))^2 + \varepsilon_1^2 + \dots + \varepsilon_K^2}{2\theta(x, t)}\right) \quad (2.1)$$

with  $\theta(x, t) = \frac{p(x, t)}{\rho(x, t)}$  being the absolute temperature.

Now, let us see how the Euler equation is derived from the Boltzmann equation. For simplicity, let us assume that molecules have no internal motion, i.e.  $K = 0$ , and therefore  $\gamma = 3$ . We also choose the BGK model as our Boltzmann equation,

$$f_t + \xi f_x = Q(f, f) \quad (2.2)$$

with  $Q(f, f) = -\frac{M-f}{\tau}$ , and  $\tau$  is the average time interval between successive particle collisions for the same particle, also known as the mean free path. From the physical constraints

of conservation of mass, momentum and energy during particle collisions, the following compatibility condition has to be satisfied,

$$\int \psi_\alpha Q(f, f) d\xi = 0$$

where  $\psi_\alpha = (1, \xi, \frac{1}{2}\xi^2)^T$ . Multiplying the Boltzmann equation (2.2) by  $\psi_\alpha$ , we obtain the macroscopic model

$$\mathbf{u}_t + \mathbf{F}(\mathbf{u})_x = 0 \quad (2.3)$$

where

$$\mathbf{u} = \begin{pmatrix} \rho \\ m \\ E \end{pmatrix} = \int_{\mathbb{R}} f(x, \xi, t) \begin{pmatrix} 1 \\ \xi \\ \frac{1}{2}\xi^2 \end{pmatrix} d\xi, \quad (2.4)$$

and

$$\mathbf{F}(\mathbf{u}) = \begin{pmatrix} F_1(\mathbf{u}) \\ F_2(\mathbf{u}) \\ F_3(\mathbf{u}) \end{pmatrix} = \int_{\mathbb{R}} f(x, \xi, t) \begin{pmatrix} \xi \\ \xi^2 \\ \frac{1}{2}\xi^3 \end{pmatrix} d\xi. \quad (2.5)$$

If  $f$  is a local Maxwellian at time  $t$ , i.e.  $f(x, \xi, t) = M(x, \xi, t)$ , we can write out the explicit form of the flux (2.5). The first component of the flux derivative is

$$(F_1)_x = \int_{\mathbb{R}} \xi M(x, \xi, t)_x d\xi = \left( \int_{\mathbb{R}} \xi M(x, \xi, t) d\xi \right)_x = m_x = (\rho v)_x. \quad (2.6)$$

Due to the equation of state and  $\gamma = 3$ , the second component of the flux derivative is

$$\begin{aligned} (F_2)_x &= \int_{\mathbb{R}} \xi^2 M(x, \xi, t)_x d\xi = \left( \int_{\mathbb{R}} \xi^2 M(x, \xi, t) d\xi \right)_x \\ &= 2E_x = 2 \left( \frac{p}{\gamma - 1} + \frac{1}{2}\rho v^2 \right)_x = (p + \rho v^2)_x. \end{aligned} \quad (2.7)$$

The above two flux terms are computed without using the Maxwellian property, that is to say that for non-equilibrium states, flux derivatives (2.6) and (2.7) are also valid. The last flux term is

$$(F_3)_x = \frac{1}{2} \int_{\mathbb{R}} \xi^3 M(x, \xi, t)_x d\xi = \frac{1}{2} \left( \int_{\mathbb{R}} \xi^3 M(x, \xi, t) d\xi \right)_x. \quad (2.8)$$

Substituting equation (2.1) into the right hand side, and changing the variable  $z = \frac{\xi - v}{\sqrt{\theta}}$ , we

have

$$\begin{aligned}
\int_{\mathbb{R}} \xi^3 M(x, \xi, t) d\xi &= \frac{\rho}{(2\pi)^{\frac{1}{2}}} \int_{\mathbb{R}} (v + z\sqrt{\theta})^3 \exp\left(-\frac{z^2}{2}\right) dz \\
&= \frac{\rho}{(2\pi)^{\frac{1}{2}}} \int_{\mathbb{R}} \left( v^3 \exp\left(-\frac{z^2}{2}\right) + 3v^2\sqrt{\theta}z \exp\left(-\frac{z^2}{2}\right) \right. \\
&\quad \left. + 3v\theta z^2 \exp\left(-\frac{z^2}{2}\right) + \theta^{3/2}z^3 \exp\left(-\frac{z^2}{2}\right) \right) dz \\
&= \rho(v^3 + 3v\theta) = v \left( \rho v^2 + 3\rho \frac{p}{\rho} \right) \\
&= v(2E + 2p). \tag{2.9}
\end{aligned}$$

Plugging (2.9) into (2.8), we obtain the third flux derivative term

$$(F_3)_x = (v(E + p))_x. \tag{2.10}$$

The three flux derivative terms (2.6), (2.7) and (2.10) provide our Euler fluxes

$$\mathbf{F}(\mathbf{u}) = \begin{pmatrix} \rho v \\ \rho v^2 + p \\ v(E + p) \end{pmatrix}.$$

Therefore, when the flow is in the equilibrium state, we can use the macroscopic model, such as the Euler system, to simulate the flow. However, in a real physical situation, gas does not necessarily stay in the local thermodynamic equilibrium (LTE) state, such as gas inside a shock or a boundary layer. Usually, we do not know the explicit form of the gas distribution function  $f$  in extremely dissipative flow regions, such as that inside a strong shock wave. What we know is the time evolution of  $f$ , through the Boltzmann equation. For this case, we can only use the microscopic model, such as the Boltzmann equation, to compute  $f$ , then use (2.4) to evaluate the macroscopic data that we are interested in.

## 2.1 Setup of the numerical scheme

We denote the  $x$ -direction computational mesh by  $I_i = [x_{i-\frac{1}{2}}, x_{i+\frac{1}{2}}]$  for  $i = 1, \dots, N$  with the center of the cell denoted by  $x_i = \frac{1}{2}(x_{i-\frac{1}{2}} + x_{i+\frac{1}{2}})$  and the size of each cell by  $\Delta x_i = x_{i+\frac{1}{2}} - x_{i-\frac{1}{2}}$ , with the maximum mesh size  $\Delta x = \max_i \Delta x_i$ . We also denote  $P^k(I)$  as the

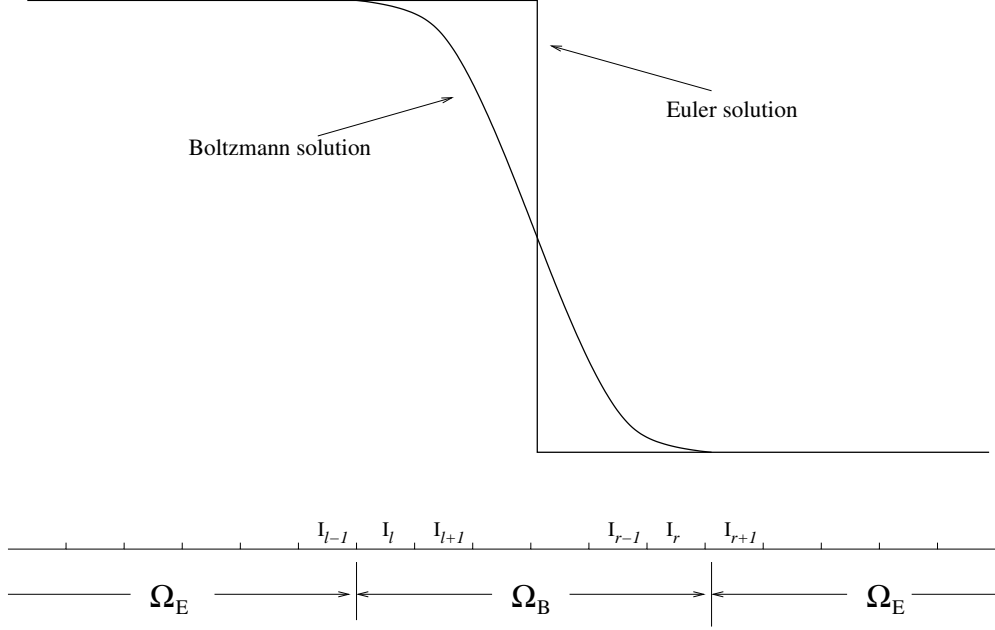


Figure 2.1: An example of domain decomposition

space of polynomials in an interval  $I$  of degree at most  $k$ . We can choose a basis of  $P^k(I_i)$  as, for example,  $\{1, \zeta_i, \dots, \zeta_i^k\}$ , where the monomials  $\zeta_i = \frac{x-x_i}{\Delta x_i}$ . The  $\xi$ -direction mesh is similarly denoted as  $J_j = [\xi_{j-\frac{1}{2}}, \xi_{j+\frac{1}{2}}]$ ,  $\xi_j = \frac{1}{2} (\xi_{j-\frac{1}{2}} + \xi_{j+\frac{1}{2}})$ , and  $\Delta \xi_j = \xi_{j+\frac{1}{2}} - \xi_{j-\frac{1}{2}}$  for  $j = 1, \dots, N_\xi$ .

We decompose the computational domain into two parts. The region where gas stays in an equilibrium state is called the Euler region, denoted by  $\Omega_E(t)$ , and the region where gas does not stay in equilibrium is called the Boltzmann region, denoted by  $\Omega_B(t)$ , see Figure 2.1. Define  $C_E(t) = \{i, \text{ such that cell } I_i \in \Omega_E \text{ at time } t\}$ , and  $C_B(t) = \{i, \text{ such that cell } I_i \in \Omega_B \text{ at time } t\}$ . For the case of Figure 2.1,  $C_E(t) = \{1, 2, \dots, l-1, r+1, r+2, \dots, N\}$  and  $C_B(t) = \{l, l+1, \dots, r-1, r\}$ . We solve the macroscale Euler system (2.3) in the Euler region and solve the microscale Boltzmann equation (2.2) in the Boltzmann region. For both regions, we use the discontinuous Galerkin method [11, 10].

We denote  $\rho_i^n(x)$  as the polynomial of  $\rho$  at time  $t^n$  in cell  $I_i$ , and  $f_{ij}^n(x, \xi)$  as the polynomial of  $f$  at time  $t^n$  in cell  $I_i \cap J_j$ . At time  $t^n$ , we have the macroscopic data  $\rho_i^n, m_i^n$  and  $E_i^n$  in the Euler region for  $i \in C_E(t^n)$ , and the microscopic data  $f_{ij}^n$  in the Boltzmann regions

for  $i \in C_B(t^n)$  and all  $j$ . If the shocks or contact discontinuities are stationary,  $\Omega_E(t)$  and  $\Omega_B(t)$ , hence  $C_E(t)$  and  $C_B(t)$ , will not change with time  $t$ . However, when the discontinuities move,  $C_E(t^{n+1})$  may be different from  $C_E(t^n)$  and  $C_B(t^{n+1})$  may be different from  $C_B(t^n)$ . If  $i \in C_B(t^{n+1})$  but  $i \in C_E(t^n)$ , i.e., if cell  $I_i$  belongs to the Euler region at time  $t^n$ , but now belongs to the Boltzmann region at time  $t^{n+1}$ , we would need to obtain microscopic data  $f_{ij}^n$  from the macroscopic data  $\rho_i^n, m_i^n$  and  $E_i^n$  by assuming a Maxwellian distribution

$$f_{ij}^n = \frac{\rho_i^n}{\sqrt{2\pi\theta_i^n}} \exp\left(-\frac{(\xi_j - v_i^n)^2}{2\theta_i^n}\right). \quad (2.11)$$

On the other hand, if  $i \in C_E(t^{n+1})$  but  $i \in C_B(t^n)$ , i.e., if cell  $I_i$  belongs to the Boltzmann region at time  $t^n$ , but now belongs to the Euler region at time  $t^{n+1}$ , we would need to obtain the macroscopic data  $\rho_i^n, m_i^n$  and  $E_i^n$  from the microscopic data  $f_{ij}^n$  by taking its moments through formula (2.4).

We now describe the discontinuous Galerkin method in each region. The  $(k+1)$ -th order accurate  $P^k$  discontinuous Galerkin scheme for the Euler system (2.3)-(2.5) is given by: Find  $\mathbf{u}^{n+1}(x)$  with each of its components in  $V_h = \{h : h|_{I_i} \in P^k(I_i), i \in C_E(t^{n+1})\}$  such that

$$\int_{I_i} \frac{\mathbf{u}^{n+1} - \mathbf{u}^n}{\Delta t} h dx - \int_{I_i} \mathbf{F}(\mathbf{u}^n) h_x dx + \widehat{\mathbf{F}}_{i+\frac{1}{2}}^n h_{i+\frac{1}{2}}^- - \widehat{\mathbf{F}}_{i-\frac{1}{2}}^n h_{i-\frac{1}{2}}^+ = 0$$

for  $h = 1, \zeta_i, \dots, \zeta_i^k, i \in C_E(t^{n+1})$ , where, e.g.  $h_{i+\frac{1}{2}}^- = h(x_{i+\frac{1}{2}}^-)$ . Notice that we have written out the scheme by a first order Euler forward time discretization for simplicity of presentation. The actual computation uses a second or third order TVD Runge-Kutta time discretization [31] which is a convex combination of two or three Euler forward operators. The numerical flux is chosen as the kinetic flux:

$$\widehat{\mathbf{F}}_{i+\frac{1}{2}} = \int_{\mathbb{R}^+} M(x_{i+\frac{1}{2}}^-, \xi, t) \begin{pmatrix} \xi \\ \xi^2 \\ \frac{1}{2}\xi^3 \end{pmatrix} d\xi + \int_{\mathbb{R}^-} M(x_{i+\frac{1}{2}}^+, \xi, t) \begin{pmatrix} \xi \\ \xi^2 \\ \frac{1}{2}\xi^3 \end{pmatrix} d\xi, \quad (2.12)$$

where the Maxwellian  $M$  is computed by using (2.1). The numerical flux (2.12) can be evaluated (see [32] for details) as

$$\widehat{\mathbf{F}}_{i+\frac{1}{2}} = \mathbf{F}_{i+\frac{1}{2}}^- + \mathbf{F}_{i+\frac{1}{2}}^+$$

for  $i = 1, \dots, l-2, r+1, \dots, N$ , with

$$\mathbf{F}_{i+\frac{1}{2}}^- = \rho_{i+\frac{1}{2}}^- \begin{pmatrix} \frac{v_{i+\frac{1}{2}}^-}{2} A(-S_{i+\frac{1}{2}}^-) + \frac{1}{2} \frac{B(S_{i+\frac{1}{2}}^-)}{\sqrt{\pi\lambda_{i+\frac{1}{2}}^-}} \\ \left( \frac{(v_{i+\frac{1}{2}}^-)^2}{2} + \frac{1}{4\lambda_{i+\frac{1}{2}}^-} \right) A(-S_{i+\frac{1}{2}}^-) + \frac{v_{i+\frac{1}{2}}^-}{2} \frac{B(S_{i+\frac{1}{2}}^-)}{\sqrt{\pi\lambda_{i+\frac{1}{2}}^-}} \\ \left( \frac{(v_{i+\frac{1}{2}}^-)^3}{4} + \frac{3}{8\lambda_{i+\frac{1}{2}}^-} v_{i+\frac{1}{2}}^- \right) A(-S_{i+\frac{1}{2}}^-) + \left( \frac{(v_{i+\frac{1}{2}}^-)^2}{4} + \frac{1}{4\lambda_{i+\frac{1}{2}}^-} \right) \frac{B(S_{i+\frac{1}{2}}^-)}{\sqrt{\pi\lambda_{i+\frac{1}{2}}^-}} \end{pmatrix},$$

and

$$\mathbf{F}_{i+\frac{1}{2}}^+ = \rho_{i+\frac{1}{2}}^+ \begin{pmatrix} \frac{v_{i+\frac{1}{2}}^+}{2} A(S_{i+\frac{1}{2}}^+) - \frac{1}{2} \frac{B(S_{i+\frac{1}{2}}^+)}{\sqrt{\pi\lambda_{i+\frac{1}{2}}^+}} \\ \left( \frac{(v_{i+\frac{1}{2}}^+)^2}{2} + \frac{1}{4\lambda_{i+\frac{1}{2}}^+} \right) A(S_{i+\frac{1}{2}}^+) - \frac{v_{i+\frac{1}{2}}^+}{2} \frac{B(S_{i+\frac{1}{2}}^+)}{\sqrt{\pi\lambda_{i+\frac{1}{2}}^+}} \\ \left( \frac{(v_{i+\frac{1}{2}}^+)^3}{4} + \frac{3}{8\lambda_{i+\frac{1}{2}}^+} v_{i+\frac{1}{2}}^+ \right) A(S_{i+\frac{1}{2}}^+) - \left( \frac{(v_{i+\frac{1}{2}}^+)^2}{4} + \frac{1}{4\lambda_{i+\frac{1}{2}}^+} \right) \frac{B(S_{i+\frac{1}{2}}^+)}{\sqrt{\pi\lambda_{i+\frac{1}{2}}^+}} \end{pmatrix},$$

where

$$A(S) = \operatorname{erfc}(S), \quad B(S) = \exp(-S^2), \quad S^\pm = v^\pm \sqrt{\lambda^\pm}, \quad \lambda = \frac{1}{2\theta},$$

and the complementary error function is defined by

$$\operatorname{erfc}(x) = \frac{2}{\sqrt{\pi}} \int_x^\infty e^{-t^2} dt.$$

At the macro-micro interface boundaries  $x_{l-\frac{1}{2}}$  and  $x_{r+\frac{1}{2}}$ , we define the fluxes as

$$\widehat{\mathbf{F}}_{l-\frac{1}{2}} = \int_{\mathbb{R}^+} M(x_{l-\frac{1}{2}}^-, \xi, t) \begin{pmatrix} \xi \\ \xi^2 \\ \frac{1}{2}\xi^3 \end{pmatrix} d\xi + \int_{\mathbb{R}^-} f(x_{l-\frac{1}{2}}^+, \xi, t) \begin{pmatrix} \xi \\ \xi^2 \\ \frac{1}{2}\xi^3 \end{pmatrix} d\xi, \quad (2.13)$$

and

$$\widehat{\mathbf{F}}_{r+\frac{1}{2}} = \int_{\mathbb{R}^+} f(x_{r+\frac{1}{2}}^-, \xi, t) \begin{pmatrix} \xi \\ \xi^2 \\ \frac{1}{2}\xi^3 \end{pmatrix} d\xi + \int_{\mathbb{R}^-} M(x_{r+\frac{1}{2}}^+, \xi, t) \begin{pmatrix} \xi \\ \xi^2 \\ \frac{1}{2}\xi^3 \end{pmatrix} d\xi. \quad (2.14)$$

Notice that the kinetic flux (2.12) is particularly suitable for the transferring of information from the micro sub-domain solution  $f$  to the macro sub-domain flux  $\widehat{\mathbf{F}}$  through upwinding via (2.13)-(2.14). However, we have also tested the simpler Lax-Friedrichs flux and have obtained similarly satisfactory results.

In the Boltzmann regions, we define the space of polynomials in a two dimensional cell  $I_i \cap J_j$  of degree at most  $k$  as

$$Q^k(I_i, J_j) = \{w : w = \sum_{k_1+k_2 \leq k} a_{k_1 k_2} \zeta_i^{k_1} \eta_j^{k_2}\}$$

with  $\zeta_i$  defined as before and  $\eta_j = \frac{\xi - \xi_j}{\Delta \xi_j}$ . The DG scheme for the Boltzmann equation (2.2) is given by: Find  $f^{n+1} \in W_h = \{w : w|_{I_i, J_j} \in Q^k(I_i, J_j), i \in C_B(t^{n+1}), j = 1, \dots, N_\xi\}$ , such that

$$\begin{aligned} \int_{I_i} \int_{J_j} \frac{f^{n+1} - f^n}{\Delta t} h dx d\xi - \int_{J_j} \xi \left( \int_{I_i} f^n h_x dx \right) d\xi + \int_{J_j} \xi_{i+\frac{1}{2}} \widehat{f}_{i+\frac{1}{2}}^n h d\xi - \int_{J_j} \xi_{i-\frac{1}{2}} \widehat{f}_{i-\frac{1}{2}}^n h d\xi \\ = \int_{I_i} \int_{J_j} Q(f^n, f^n) h dx d\xi. \end{aligned}$$

for  $h = \zeta_i^{k_1} \eta_j^{k_2}$  with  $k_1 + k_2 \leq k$ . Notice that we have again written out the scheme by a first order Euler forward time discretization for simplicity of presentation while the actual computation uses a second or third order TVD Runge-Kutta time discretization, which is synchronized with the time discretization in the macro sub-domains. The numerical fluxes are chosen as simple upwinding

$$\widehat{f}_{i+\frac{1}{2}} = \begin{cases} f_{i+\frac{1}{2}}^- & \text{if } \xi \geq 0, \\ f_{i+\frac{1}{2}}^+ & \text{if } \xi < 0. \end{cases}$$

At the macro-micro interface boundary  $x_{l-\frac{1}{2}}$ , the numerical flux for  $\xi > 0$  is given as

$$f(x_{l-\frac{1}{2}}, \xi, t) = M(x_{l-\frac{1}{2}}, \xi, t)$$

where the right hand side is the local Maxwellian corresponding to the macroscopic state at  $x_{l-\frac{1}{2}}$ . Notice that we have assumed the ansatz of an equilibrium Maxwellian to transfer information from the macro sub-domain to the micro sub-domain. The interface boundary condition at the micro-macro boundary  $x_{r+\frac{1}{2}}$  can be handled similarly.

## 2.2 Numerical examples

We use a very accurate and essentially non-oscillatory fifth order WENO scheme [22] to compute the BGK equation (2.2) throughout the computational domain with a uniform

refined mesh of  $800 \times 100$  grid points, to obtain a reference “exact” solution. For all the test examples in this subsection, we compute solutions to a final time  $t = 0.5$ . The theoretical domain in  $\xi$  is  $(-\infty, \infty)$ . In our numerical experiment, we choose the domain to be  $[\max_x v - L, \max_x v + L]$ , with  $L$  big enough such that the distribution function  $f$  is negligibly small at the artificial  $\xi$  boundaries for all relevant time  $t$ . For all our test examples,  $L = 20$  is suitable. We divide this domain into  $N_\xi = 100$  uniform cells and this seems to be able to provide enough resolution for our test problems.

We have tested the following three examples.

- **Stationary Shock.** Our first example is a stationary shock problem. The initial condition is given by:

$$(\rho, v, p) = \begin{cases} (1.1428, -1.75, 1.5) & \text{if } x < 0, \\ (1., -2., 1.) & \text{if } x \geq 0. \end{cases} \quad (2.15)$$

Figure 2.2 provides the density plots by using the second order accurate  $P^1$  (left) and the third order accurate  $P^2$  (right) discontinuous Galerkin methods on both the Euler and the Boltzmann regions with uniform mesh sizes  $\Delta x = 0.1, 0.05$  and  $0.025$  for the relaxation parameter  $\tau = 10^{-2}$  in the BGK model. We divide the domain into the micro and macro sub-domains as  $\Omega_B = [-0.25, 0.25]$ , and  $\Omega_E = [-0.5, -0.25] \cup [0.25, 0.5]$ . Figure 2.3 contains density plots for the smaller relaxation parameter  $\tau = 10^{-3}$  in the BGK model. The left picture is the result by using the  $P^1$  DG method with uniform mesh sizes  $\Delta x = 0.05, 0.025$  and  $0.0125$ , and the right picture is the result by using  $P^2$  DG method with uniform meshes  $\Delta x = 0.1, 0.05$  and  $0.025$ . In this case, we divide the domain into the micro and macro sub-domains as  $\Omega_B = [-0.1, 0.1]$ , and  $\Omega_E = [-0.5, -0.1] \cup [0.1, 0.5]$ . In both Figures 2.2 and 2.3, we can clearly see that the DDM-DG numerical solutions converge to the exact reference solution with a grid refinement. There are some oscillations in Figure 2.3 when the mesh in the micro-domain is not refined enough to resolve the sharp gradient, since we have not used any limiters in the calculation. However, despite these oscillations, it is still clear that

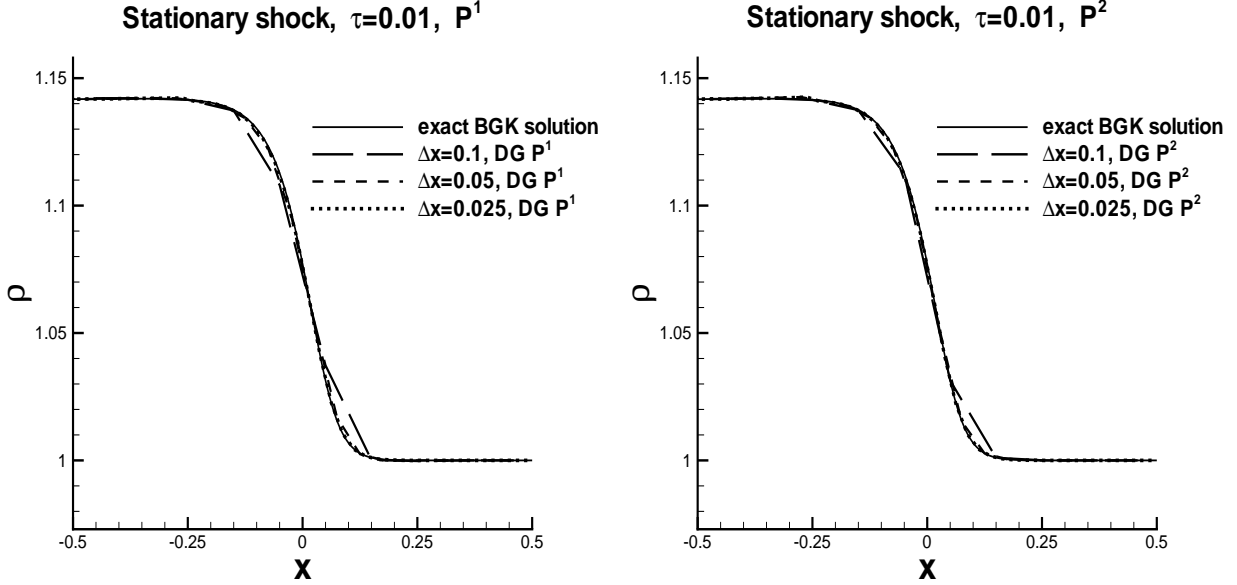


Figure 2.2: Stationary shock. Density  $\rho$ .  $\tau = 10^{-2}$ . The exact BGK solution versus the DDM-DG solution with  $\Delta x = 0.1, 0.05$ , and  $0.025$ . Left: DG  $P^1$ . Right: DG  $P^2$ .

the DDM-DG numerical solutions converge to the exact reference solution with a grid refinement.

- **Moving Contact Discontinuity.** The second example is a moving contact discontinuity problem with a moving speed 0.5. The initial condition is:

$$(\rho, v, p) = \begin{cases} (1, 0.5, 0.5) & \text{if } x < 0, \\ (0.6, 0.5, 0.5) & \text{if } x \geq 0. \end{cases} \quad (2.16)$$

Since the location of discontinuity is moving with speed 0.5, the macro and micro sub-domains must also change with time  $t$  and we use (2.11) or (2.4) to compute the necessary data when such change happens. Figure 2.4 plots the density for  $\tau = 10^{-2}$ , by using DG  $P^1$  (left) with uniform mesh sizes  $\Delta x = 0.075, 0.0375$  and  $0.01875$  and DG  $P^2$  (right) with mesh sizes  $\Delta x = 0.15, 0.075$  and  $0.0375$ . In this case, the Boltzmann region is a moving region defined as  $\Omega_B = [0.5t - 0.25, 0.5t + 0.25]$ . Figure 2.5 plots the density for  $\tau = 10^{-3}$  by using DG  $P^1$  (left) with uniform mesh sizes  $\Delta x = 0.0375, 0.01875$  and  $0.009375$ , and DG  $P^2$  (right) with mesh sizes  $\Delta x = 0.075, 0.0375$  and  $0.01875$ . The Boltzmann region in this case is  $\Omega_B = [0.5t - 0.1, 0.5t + 0.1]$ . We can clearly see that

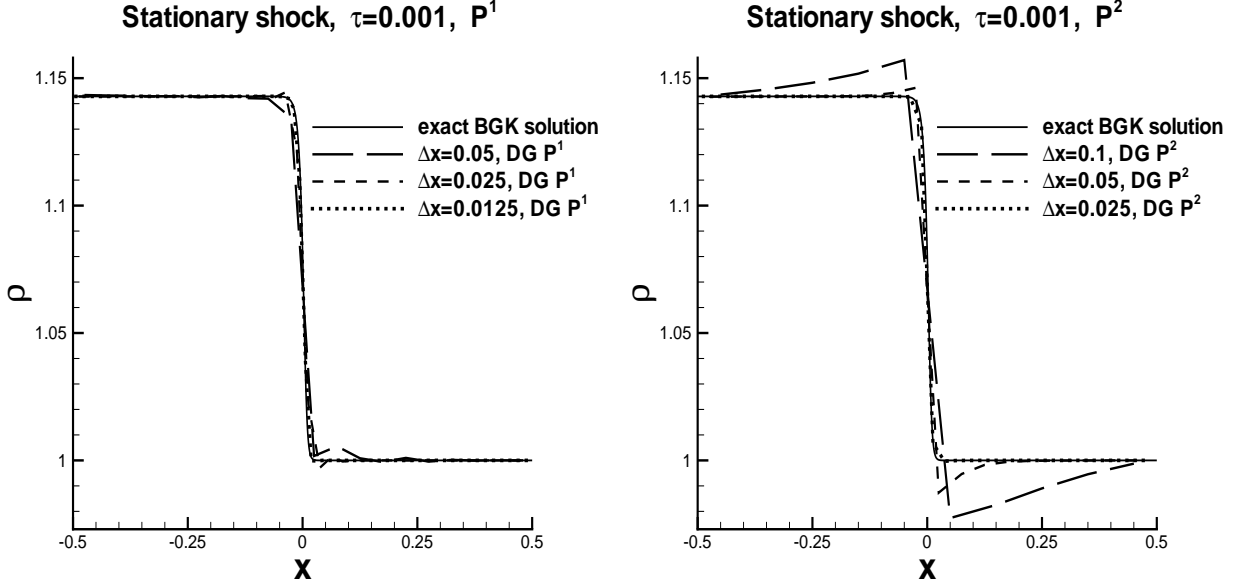


Figure 2.3: Stationary shock. Density  $\rho$ .  $\tau = 10^{-3}$ . The exact BGK solution versus the DDM-DG solution. Left: DG  $P^1$  with  $\Delta x = 0.05, 0.025$  and  $0.0125$ . Right: DG  $P^2$  with  $\Delta x = 0.1, 0.05$  and  $0.025$ .

the DDM-DG numerical solutions converge to the exact reference solution with a grid refinement.

- **Sod's Shock Tube Problem.** The last example is the Sod's shock tube problem with the initial condition

$$(\rho, v, p) = \begin{cases} (\rho_l, v_l, p_l) = (1, 0, 1) & \text{if } x < 0; \\ (\rho_r, v_r, p_r) = (0.125, 0, 0.1) & \text{if } x \geq 0. \end{cases} \quad (2.17)$$

Notice that the solution consists of a shock, a contact discontinuity and a rarefaction wave as time goes on, and the locations of the four interface points  $(x_1, x_2, x_3, x_4)$  (see Figure 2.6) are all initially at  $x = 0$  and they move with the following speeds (see [30] for the derivation)

$$\begin{aligned} v_1 &= v_l - c_l, \\ v_2 &= v_l + c_l h_1(x^*) - \sqrt{\gamma e^{-x^*} p_l / (f_1(x^*) \rho_l)}, \\ v_3 &= v_l + c_l h_1(x^*), \\ v_4 &= \frac{\rho_r v_r - e^z f_1(x^*) \rho_l (v_l + c_l h_1(x^*))}{\rho_r - e^z f_1(x^*) \rho_l}, \end{aligned} \quad (2.18)$$

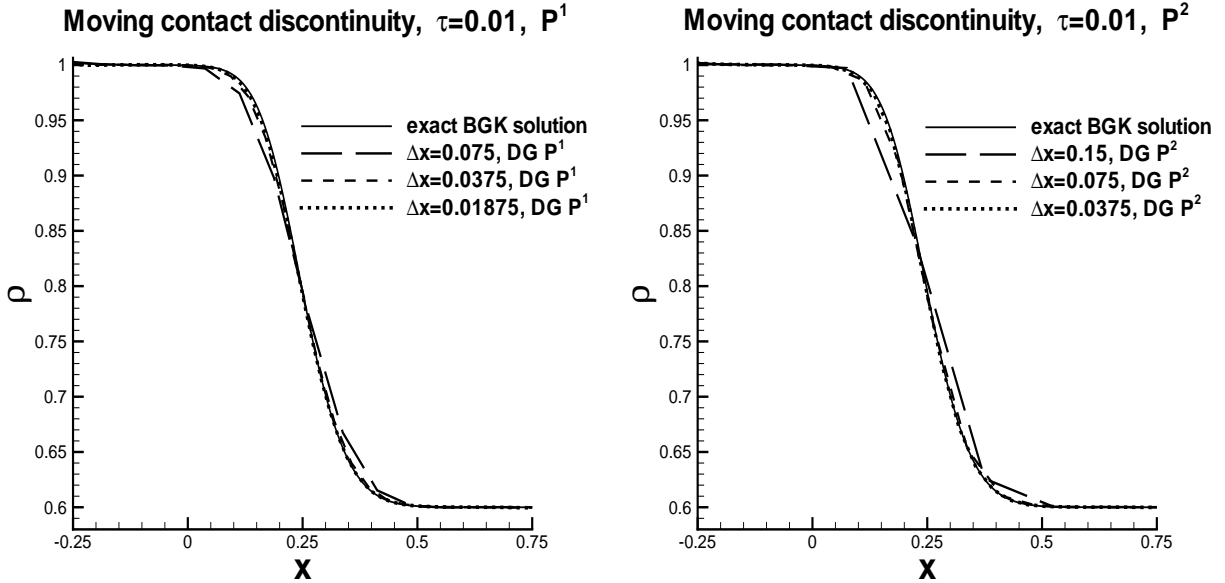


Figure 2.4: Moving contact discontinuity problem. Density  $\rho$ .  $\tau = 10^{-2}$ . The exact BGK solution versus the DDM-DG solution. Left: DG  $P^1$  with  $\Delta x = 0.075, 0.0375$  and  $0.01875$ . Right: DG  $P^2$  with  $\Delta x = 0.15, 0.075$  and  $0.0375$ .

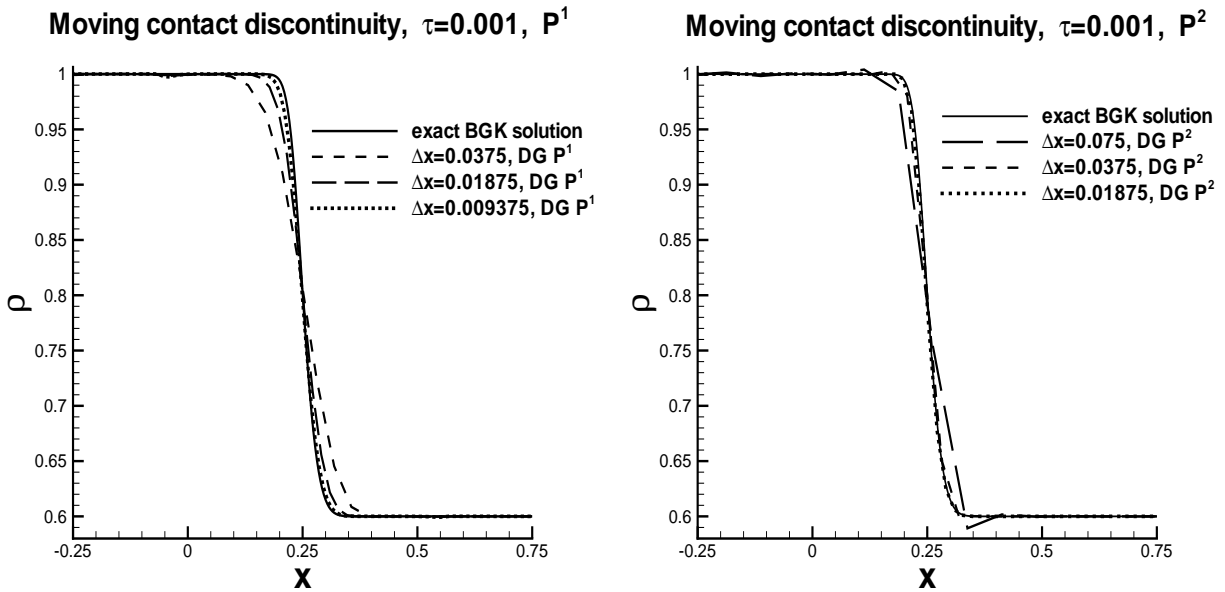


Figure 2.5: Moving contact discontinuity problem. Density  $\rho$ .  $\tau = 10^{-3}$ . The exact BGK solution versus the DDM-DG solution. Left: DG  $P^1$  with  $\Delta x = 0.0375, 0.01875$  and  $0.009375$ . Right: DG  $P^2$  with  $\Delta x = 0.075, 0.0375$  and  $0.01875$ .

respectively, where

$$h_1(x) = \begin{cases} \frac{2}{\gamma-1}(1 - e^{-\tau x}), & \text{if } x \geq 0, \\ \frac{2\sqrt{\tau}}{\gamma-1} \frac{1-e^{-x}}{\sqrt{1+\beta e^{-x}}}, & \text{if } x \leq 0, \end{cases}$$

$$f_1(x) = \begin{cases} e^{-x/\gamma}, & \text{if } x \geq 0, \\ \frac{\beta+e^x}{1+\beta e^x}, & \text{if } x \leq 0, \end{cases}$$

with  $c_l = \sqrt{\gamma p_l / \rho_l}$ ,  $\tau = \frac{\gamma-1}{2\gamma}$ , and  $\beta = \frac{\gamma+1}{\gamma-1}$ .  $x^*$  in equation (2.18) is the solution of the following equation

$$h_1(x) + \sqrt{\frac{p_r \rho_l}{p_l \rho_r}} h_1\left(x + \log \frac{p_r}{p_l}\right) - \frac{v_r - v_l}{c_l} = 0.$$

$z$  in equation (2.18) is given by

$$z = \log \frac{\rho_r f_1(x^* + \log \frac{p_r}{p_l})}{\rho_l f_1(x^*)}.$$

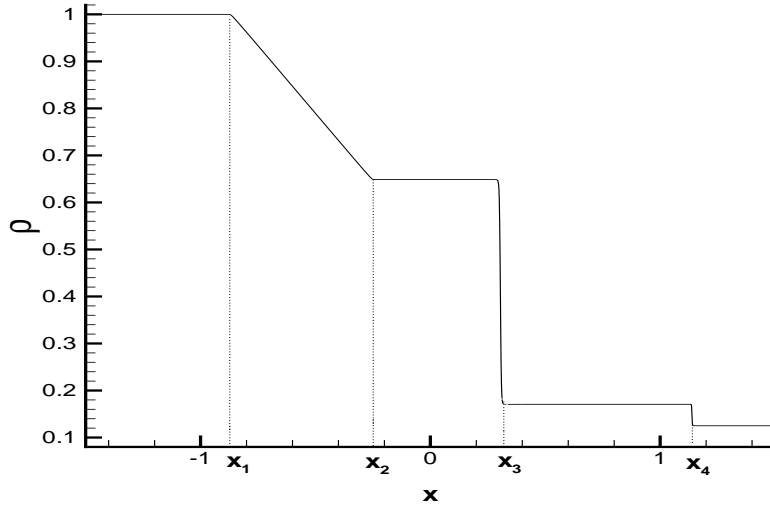


Figure 2.6: Exact Euler solution for the Sod's shock tube problem.

According to the information of the exact Euler solution, we divide the region such that the micro sub-domains are  $\Omega_B = [x_1 - 0.2, x_2 + 0.2] \cup [x_3 - 0.3, x_3 + 0.3] \cup [x_4 - 0.1, x_4 + 0.1]$  for  $\tau = 10^{-2}$ , and  $\Omega_B = [x_1 - 0.05, x_2 + 0.05] \cup [x_3 - 0.1, x_3 + 0.1] \cup [x_4 - 0.04, x_4 + 0.04]$  for  $\tau = 10^{-3}$ , where  $x_i = v_i t$  with  $v_i$  given by (2.18). Figure 2.7 shows the numerical results for  $\tau = 10^{-2}$  with mesh sizes  $\Delta x = 0.15, 0.075$  and  $0.0375$ . The left picture in

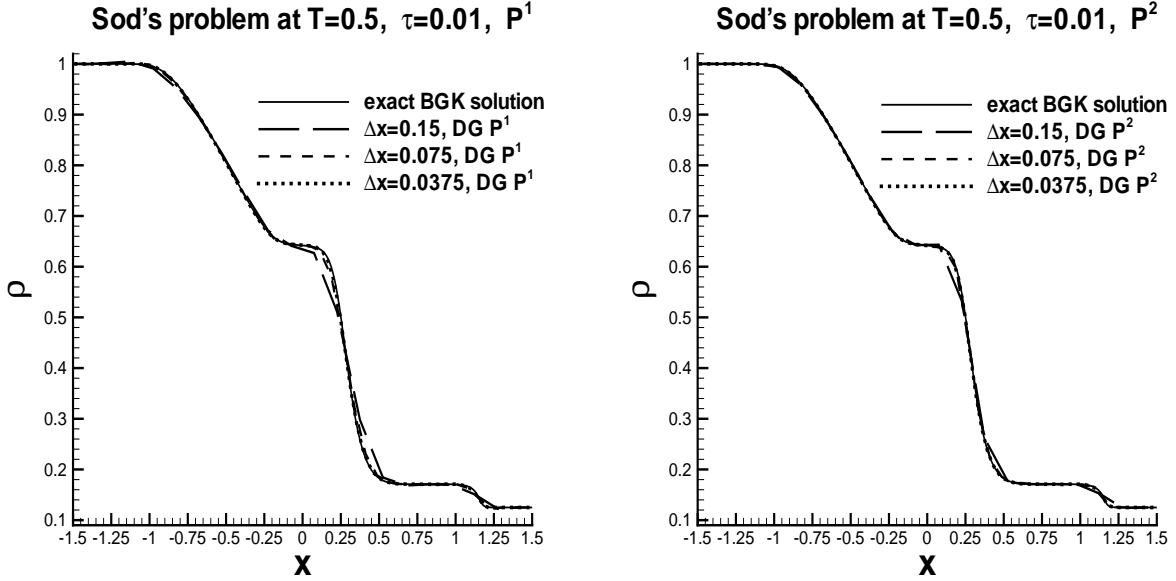


Figure 2.7: Sod's Shock tube problem. Density  $\rho$ .  $\tau = 10^{-2}$ . The exact BGK solution versus the DDM-DG solution. Left: DG  $P^1$  with  $\Delta x = 0.15, 0.075$  and  $0.0375$ . Right: DG  $P^2$  with  $\Delta x = 0.15, 0.075$  and  $0.0375$ .

Figure 2.7 is the result of using DG  $P^1$ , and the right one is the result of using DG  $P^2$ . Figure 2.8 contains the results for  $\tau = 10^{-3}$ . The left one is the result by using DG  $P^1$  with  $\Delta x = 0.075, 0.0375$  and  $0.01875$ , and the right one is the result by using DG  $P^2$  with  $\Delta x = 0.15, 0.075$  and  $0.0375$ . We can clearly see that the DDM-DG numerical solutions converge to the exact reference solution with a grid refinement.

### 3 Semiconductor device simulation for a silicon diode

In this section, we apply the DDM-DG method to solve a silicon diode problem in semiconductor device simulations. The macro models are the hydrodynamic (HD) and high field (HF) models, and the micro model is the kinetic model. These models have been simulated and compared in [6] using a fifth order WENO scheme [22]. A domain decomposition method coupling these models have also been attempted in [6], however the kinetic model is used in the whole computational domain to obtain the necessary interface data for the macro sub-domain using the HF model. This approach can verify the applicability of the HF model

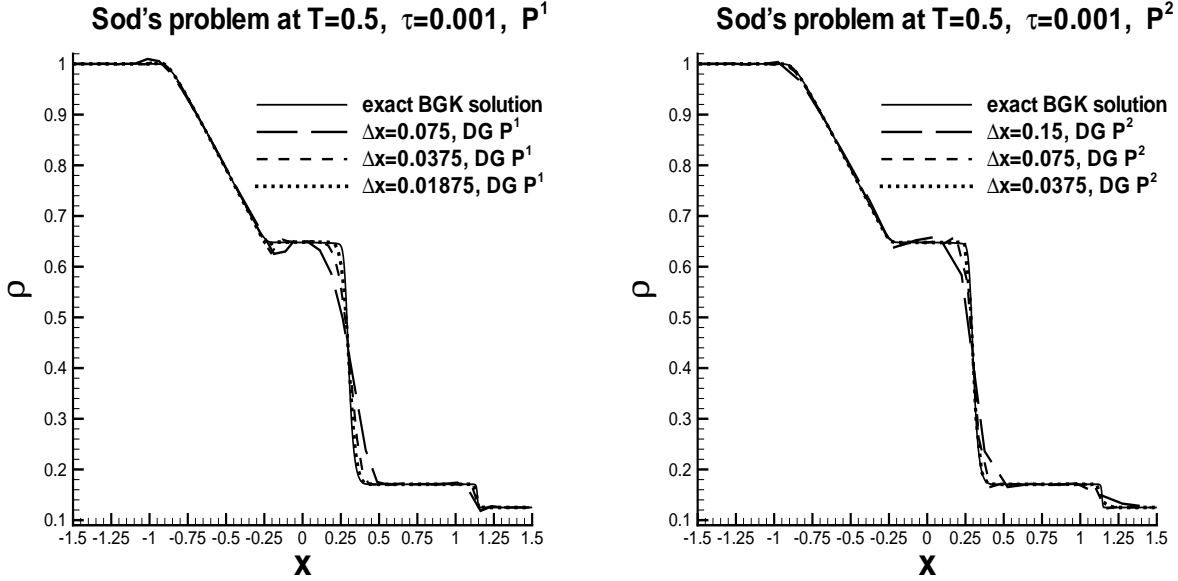


Figure 2.8: Sod's Shock tube problem. Density  $\rho$ .  $\tau = 10^{-3}$ . The exact BGK solution versus the DDM-DG solution. Left: DG  $P^1$  with  $\Delta x = 0.075, 0.0375$  and  $0.01875$ . Right: DG  $P^2$  with  $\Delta x = 0.15, 0.075$  and  $0.0375$ .

in this sub-domain, but cannot achieve a cost-reduction of utilizing the costly kinetic model only in small sub-domains. The difficulty in [6] preventing a full domain decomposition is the transfer of information from the macro HF model to the micro kinetic model, at a low doping interface where the distribution function is far from Maxwellian and also significantly different from the ansatz used to obtain the HF model. This difficulty is overcome in the current paper by using a different transferring mechanism.

We will describe the three models in next subsection, but we point out here that the macro models involve second derivative heat conduction terms, hence a local discontinuous Galerkin (LDG) method [14] is used. The diode problem also involves a self-consistent Poisson equation, which is discretized by the LDG method as well. We refer to [25] for more details of using DG and LDG methods for semi-conductor device simulations. This unified discontinuous Galerkin methodology for different components in device simulation is potentially viable for efficient  $h$ - $p$  adaptivity and parallel implementation.

### 3.1 Kinetic, hydrodynamic, and high field models

The following models are used in this paper.

- The kinetic model

The microscopic model is the Boltzmann equation of the following form [6]

$$\frac{\partial f(x, \xi, t)}{\partial t} + \xi \frac{\partial f(x, \xi, t)}{\partial x} - \frac{e}{m} E(x, t) \frac{\partial f(x, \xi, t)}{\partial \xi} = \frac{n(x, t)M(\xi) - f(x, \xi, t)}{\tau}, \quad (3.1)$$

where  $f$  is the distribution function (scaled probability density function),  $x$  the spatial variable,  $\xi$  the velocity in phase space,  $m$  the effective electron mass,  $e$  the electron charge unit, and

$$M(\xi) = \frac{1}{\sqrt{2\pi\theta}} e^{-\xi^2/2\theta} \quad (3.2)$$

is a Maxwellian, with

$$\theta = \frac{k_b}{m} T_0, \quad (3.3)$$

where  $k_b$  is the Boltzmann constant and  $T_0$  the lattice temperature. The concentration  $n(x, t)$  is obtained by

$$n(x, t) = \int_{\mathbb{R}} f(x, \xi, t) d\xi. \quad (3.4)$$

Also, the electric field  $E(x, t)$  is obtained by solving the coupled potential equation,

$$E(x, t) = -\phi_x, \quad (\varepsilon\phi_x)_x = e(n - n_d). \quad (3.5)$$

The boundary conditions are given as follows:  $\phi = \phi_0 = \frac{kT_0}{e} \ln(\frac{n_d}{n_i})$  at the left boundary with  $n_i = 1.4 \times 10^{10} \text{ cm}^{-3}$ , and  $\phi = \phi_0 + v_{bias}$  at the right boundary for potential.  $\varepsilon$  is the dielectric constant,  $n_d$  the doping,  $v_{bias}$  the voltage bias, and the relaxation parameter  $\tau$  is computed by  $\tau = \frac{m\mu}{e}$ , here  $\mu$  is the mobility:

$$\mu(E) = 2\mu_0 / [1 + \sqrt{1 + 4(\mu_0|E|/v_d)^2}], \quad (3.6)$$

where

$$\mu_0 = 0.14 \mu \text{ m}^2 / (\text{Vps}), \quad v_d = 0.11 \mu \text{ m} / \text{ps}.$$

$v_d$  here is taken to be the maximum of the velocity in the kinetic run with  $vbias = 1.0$  and  $\mu = 0.14$ .

- The hydrodynamic (HD) model

One of the macroscopic models we use is the hydrodynamic (HD) model [21], consisting of the conservation of particle number  $n$

$$n_t + (nv)_x = 0, \quad (3.7)$$

conservation of momentum  $p$

$$p_t + \left( pv + \frac{nk_b T}{m} \right)_x = -\frac{e}{m} n E - \frac{p}{\tau_p}, \quad (3.8)$$

and conservation of energy  $w$

$$w_t + \left( vw + \frac{nvk_b T}{m} \right)_x = -\frac{e}{m} nv E - \frac{w - \frac{w_0}{m}}{\tau_w} + \left( \frac{\kappa n T_x}{m} \right)_x, \quad (3.9)$$

where  $v = \frac{p}{n}$  is the velocity,  $T$  the temperature,  $\kappa = \frac{3k_b^2 T_0}{2e}$  the thermal conductivity coefficient governed by the Wiedemann-Franz law, and  $w_0 = \frac{3}{2} nk_b T_0$  denotes the rest energy. These equations are coupled to the electrostatic equation (3.5) defining  $E$ . The expressions  $\tau_p$  and  $\tau_w$  are standard momentum and energy relaxation expressions

$$\tau_p = \frac{m T_0 \mu}{e T}, \quad \tau_w = \frac{3k_b T_0}{2e V_s^2} \cdot \frac{\mu T}{T_0 + T} + \frac{\tau_p}{2}.$$

- The high-field (HF) model

This model is developed in [8] by the asymptotic expansion methods (Chapman-Enskog) for the kinetic formulation of the problem (3.1)-(3.5), under strong forcing scaling assumptions. The model can be written as follows:

$$n_t + J_x = 0,$$

where  $J = J_{hyp} + J_{vis}$ , and  $J_{hyp} = -\mu n E + \tau \mu \left( \frac{e}{\epsilon} \right) n (-\mu n E + \omega)$ ,  $J_{vis} = -\tau [n(\theta + 2\mu^2 E^2)]_x + \tau \mu E (\mu n E)_x$ . For our current one-dimensional case,  $\omega$  is taken to be a constant  $\omega = (\mu n E)|_{x=0}$ .

### 3.2 DDM-DG numerical scheme and simulation results

First we briefly describe the LDG method, using the HD model (3.7)-(3.9) and (3.5) as an example. For more details of the DG and LDG methods, including stability analysis and error estimates, we refer to [14, 15] and references therein. The idea of the LDG method is to rewrite PDEs containing higher order spatial derivatives into a larger system containing only first order spatial derivatives. Thus the HD model can be written as

$$\begin{cases} n_t + (nv)_x = 0, \\ p_t + (pv + \frac{nk_b T}{m})_x = -\frac{e}{m}nE - \frac{p}{\tau_p}, \\ w_t + (vw + \frac{nvk_b T}{m})_x = -\frac{e}{m}nvE - \frac{w - w_0}{\tau_w} + (\frac{\kappa n}{m}q)_x, \\ q - T_x = 0, \\ \varepsilon r_x = e(n - n_d), \\ r - \phi_x = 0. \end{cases} \quad (3.10)$$

We can then *formally* use the same DG method for the first order PDE to solve (3.10). The numerical fluxes are chosen as follows: the fluxes of the terms  $(nv)$ ,  $(pv + \frac{nk_b T}{m})$  and  $(vw + \frac{nvk_b T}{m})$  are chosen as the Lax-Friedrichs fluxes. Fluxes for  $q$  in the third equation and  $T$  in the fourth equation are chosen as the “alternate” fluxes  $\hat{q} = q^-$  and  $\hat{T} = T^+$  (the “-” and “+” can also be reversed), see [14]. Notice that the auxiliary variable  $q$  can be locally solved from the fourth equation in (3.10) and substituted into the third equation. This is the reason the method is called the “local” discontinuous Galerkin method and this also distinguishes LDG from the classical mixed finite element methods, where the auxiliary variable  $q$  must be solved from a global system. In the fifth and sixth equations in (3.10), which describe the Poisson equation, we choose numerical fluxes  $\hat{r}$  and  $\hat{\phi}$  as  $\hat{\phi} = \phi^-$ ,  $\hat{r} = r^+ - [\phi]$  (the “-” and “+” can also be reversed), where  $[\phi]$  denotes the jump  $\phi^+ - \phi^-$ . Again, the auxiliary variable  $r$  can be locally solved from the sixth equation in (3.10) and substituted into the fifth equation, resulting in a system for  $\phi$  which can be solved by standard linear solvers.

The device we consider for this paper is the one dimensional silicon  $n^+ - n - n^+$  diode of length  $0.8\mu m$ . The device used is as follows:  $x \in [0, 0.8]$ ; the doping is defined by  $n_d(x) = 10^6/\mu m^3$  in  $0 \leq x \leq 0.175$  and in  $0.625 \leq x \leq 0.8$ , and by  $n_d(x) = 2 \times 10^3/\mu m^3$  in

$0.225 \leq x \leq 0.575$ , with a smooth intermediate transition. For the kinetic model, the velocity space is artificially cut at  $-L \leq \xi \leq L$ , where we monitor to ensure that  $f(x, \xi, t)$  is always negligibly small at the boundary  $\xi = \pm L$  for the final steady state results. Through numerical experiments, we have determined that it is more than enough in all our runs to use  $L = 3.5$ .

We divide the whole domain into non-overlapping sub-domains

$$\Omega_{HD} = [0, A] \cup [0.8 - A, 0.8], \quad \Omega_{HF} = [B, 0.8 - B], \quad \Omega_K = [A, B] \cup [0.8 - B, 0.8 - A].$$

We apply the HD model in  $\Omega_{HD}$ , the HF model in  $\Omega_{HF}$ , and the kinetic model in  $\Omega_K$ .

At the interfaces  $x = A$  and  $x = 0.8 - A$ , the boundary conditions for the HD model from the kinetic region are given by integrating  $f(x, \xi, t)$  with respect to  $\xi$  over  $\mathbb{R}$ . For example, at  $x = A$ , the left is the HD region with data  $(n, p, w)|_{x=A^-}$  and the right is the kinetic region with data  $f(A^+, \xi, t)$ , thus the boundary condition at  $x = A$  for the HD model is given by

$$\left( \begin{array}{c} n \\ p \\ w \end{array} \right) \Big|_{x=A^+} = \int_{\mathbb{R}} f(A^+, \xi, t) \left( \begin{array}{c} 1 \\ \xi \\ \frac{3}{2}\xi^2 - 2v\xi + v^2 \end{array} \right) d\xi.$$

The boundary condition at  $x = A$  for the kinetic region are supplied from the HD model. However, the ansatz for the distribution function is not Maxwellian but the shape of the micro simulation at the boundary adjusted by the macro moment data, namely

$$f(A^-, \xi, t) = cf(A^+, \frac{\xi - d}{e}, t), \tag{3.11}$$

where the constants  $c$ ,  $d$ , and  $e$  are determined by requiring

$$\left( \begin{array}{c} n \\ p \\ w \end{array} \right) \Big|_{x=A^-} = \int_{\mathbb{R}} f(A^-, \xi, t) \left( \begin{array}{c} 1 \\ \xi \\ \frac{3}{2}\xi^2 - 2v\xi + v^2 \end{array} \right) d\xi.$$

This is to say that we are keeping the general shape of the distribution function  $f$  obtained from the micro sub-domain, and adjust its height and shift and scale it in the velocity space to match the first three moments from the macro sub-domain. We could also require the new  $f$  to be the closest, in some given norm such as the  $L^2$  norm, to the original  $f$  in the

micro sub-domain, with the constraint that its first three moments match those from the macro sub-domain. We have adopted the approach in (3.11) because of its simplicity and good numerical performance in our test cases.

Likewise, at the interfaces of  $x = B$  and  $x = 0.8 - B$ , we need to provide boundary conditions for the HF model and the kinetic model from each other. For example, at the interface point  $x = B$ , the left region is the kinetic model with data  $f(B^-, \xi, t)$ , and the right region is the HF model with data  $n(B^+)$ . The boundary condition for the HF model at  $x = B$  is simply given by taking the first moment of  $f$ :

$$n(B^-) = \int_{\mathbb{R}} f(B^-, \xi, t) d\xi;$$

the boundary condition for the kinetic model is given by

$$f(B^+, \xi, t) = cf(B^-, \xi, t),$$

i.e. by a simple adjustment of the height of  $f$ , where the constant  $c$  is determined by requiring

$$n(B^+) = \int_{\mathbb{R}} f(B^+, \xi, t) d\xi.$$

We perform the simulation for  $vbias = 1.0V$ , with other parameters given as  $m = 0.065 \times 0.9109(10^{-30}Kg)$ ,  $e = 0.1602(10^{-18}C)$ ,  $k_b = 0.138046 \times 10^{-4}(10^{-18}J/Kelvin)$ ,  $\varepsilon = 13.2 \times 8.85418$ , and  $T_0 = 300K$ . The domain is decomposed with  $A = 0.15$  and  $B = 0.3$ .

In the numerical simulation, we perform a long time integration until a steady state is reached. We use the piecewise linear DG and LDG schemes on a uniform grid in  $x$  with 160 points, and in  $\xi$  with 100 points. The complete system is advanced with the second order total variation diminishing (TVD) Runge-Kutta method [31] in time. Figure (3.1) gives the plots of the concentration  $n$  and electric field  $E$ . We can clearly see that the DDM-DG provides very good numerical results in agreement with the results obtained by using globally the kinetic model.

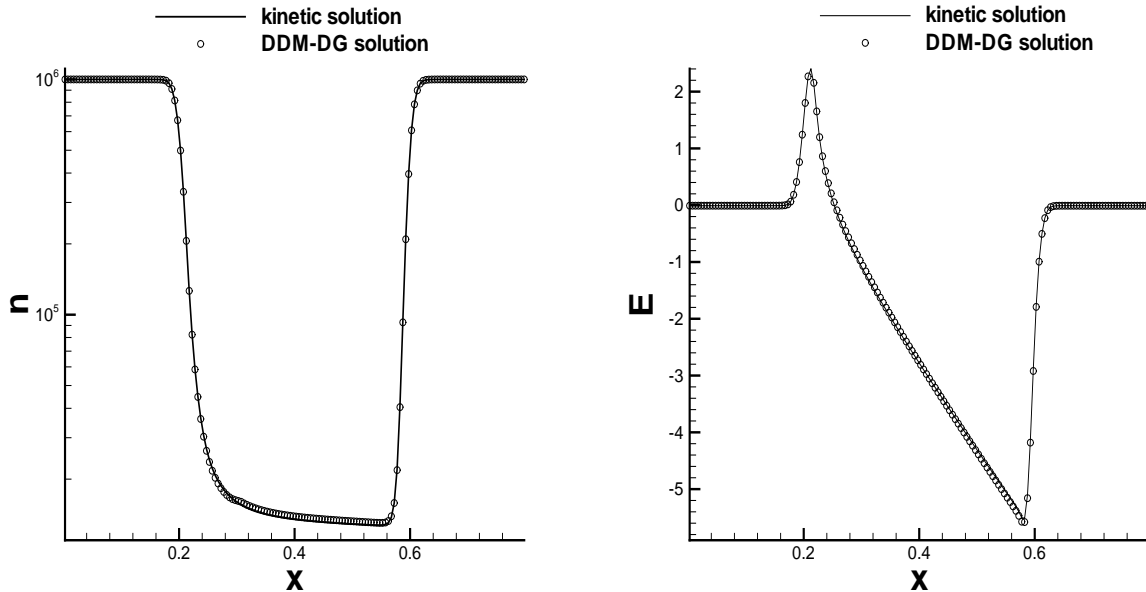


Figure 3.1: The global kinetic simulation (solid line) versus the DDM-DG solution (circles). Left: the concentration  $n$ ; right: the electric field  $E$ .

## 4 Concluding remarks

We have developed and tested a domain decomposition method for solving multiscale problems involving both micro kinetic models and macro hydrodynamic and high field models. The numerical method used for both the micro and the macro problems is the discontinuous Galerkin method. Termed DDM-DG method, this approach works effectively for our test problems in both gas dynamics flows and semiconductor device simulation of a silicon diode. A major advantage of our approach is the adoption of a DG and local discontinuous Galerkin (LDG) framework for all derivative terms in the system, thereby allowing the most effective transfer of information between the micro and the macro sub-domains through the numerical fluxes. One major findings of this paper is the treatment of the information transfer from macro to micro sub-domains. Instead of the usual approach of utilizing an ansatz such as a Maxwellian, we use the computed distribution function from the micro sub-domain and simply adjust its height and shift and scale its velocity to match the macro data. The numerical performance of this approach is very good, both for gas dynamics problems in-

volving stationary shocks and moving contacts, and for shock tube problems where a single discontinuity becomes three different waves; and for the semi-conductor device simulations of a silicon diode. The results of our DDM-DG method are in good agreement with reference solutions obtained by using the micro model throughout the computational domain. Future work will include more tests for other systems, multi-dimensions, adaptive meshes, effective identification of the macro and micro sub-domains, and more study on the transferring of information between the micro and macro sub-domains.

## References

- [1] F.F. Abraham, J.Q. Broughton, N. Bernstein and E. Kaxiras, *Concurrent coupling of length scales: methodology and application*, Phys. Rev. B, 60 (1999), pp.2391-2402.
- [2] F.F. Abraham, J.Q. Broughton, N. Bernstein and E. Kaxiras, *Spanning the continuum to quantum length scales in a dynamics simulation of brittle fracture*, Europhys. Lett., 44 (1998), pp.783-787.
- [3] J.F. Bourgat, P. Le Tallec, B. Perthame and Y. Qiu, *Coupling Boltzmann and Euler equations without overlapping*, Domain Decomposition Methods in Science and Engineering, Am. Math. Soc., 1992, pp.377-398.
- [4] J.F. Bourgat, P. Le Tallec and M. Tidriri, *Coupling Boltzmann and Navier-Stokes equations by friction*, J. Comput. Phys., 127 (1996), pp.227-245.
- [5] C. Cercignani, I. Gamba, J. Jerome and C.-W. Shu, *Applicability of the high field model: a preliminary numerical study*, VLSI Design, 8 (1998), pp.275-282.
- [6] C. Cercignani, I. Gamba, J. Jerome and C.-W. Shu, *Device benchmark comparisons via kinetic, hydrodynamic, and high-field models*, Comput. Methods Appl. Mech. Eng., 181 (2000), pp.381-392.

- [7] C. Cercignani, I. Gamba, J. Jerome and C.-W. Shu, *A domain decomposition method for silicon devices*, Transport Theory and Statistical Physics, 29 (2000), pp.525-536.
- [8] C. Cercignani, I.M. Gamba and C.D. Levermore, *High field approximations to Boltzmann-Poisson system boundary conditions in a semiconductor*, Appl. Math. Lett., 10 (1997), pp.111-117.
- [9] J.A. Carrillo, I.M. Gamba, A. Majorana and C.-W. Shu, *A WENO-solver for the transients of Boltzmann-Poisson system for semiconductor devices. Performance and comparisons with Monte Carlo methods*, J. Comput. Phys., 184 (2003), pp.498-525.
- [10] B. Cockburn, S. Hou and C.-W. Shu, *The Runge-Kutta local projection discontinuous Galerkin finite element method for conservation laws IV: the multidimensional case*, Math. Comp., 54 (1990), pp.545-581.
- [11] B. Cockburn, S.-Y. Lin and C.-W. Shu, *TVB Runge-Kutta local projection discontinuous Galerkin finite element method for conservation laws III: one dimensional systems*, J. Comput. Phys., 84 (1989), pp.90-113.
- [12] B. Cockburn and C.-W. Shu, *TVB Runge-Kutta local projection discontinuous Galerkin finite element method for conservation laws II: general framework*, Math. Comp., 52 (1989), pp.411-435.
- [13] B. Cockburn and C.-W. Shu, *The Runge-Kutta discontinuous Galerkin method for conservation laws V: multidimensional systems*, J. Comput. Phys., 141 (1998), pp.199-224.
- [14] B. Cockburn and C.-W. Shu, *The local discontinuous Galerkin method for time-dependent convection-diffusion systems*, SIAM J. Numer. Anal., 35 (1998), pp.2440-2463.
- [15] B. Cockburn and C.-W. Shu, *Runge-Kutta discontinuous Galerkin methods for convection-dominated problems*, J. Sci. Comput., 173 (2001), pp.173-261.

- [16] W. E and B. Engquist, *The heterogeneous multi-scale methods*, Comm. Math. Sci., 1 (2003), pp.87-132.
- [17] W. E, X. Li and E. Vanden-Eijnden, *Some recent progress in multiscale modeling*, in Multiscale Modeling and Simulation, S. Attinger and P. Koumoutsakos, Editors, Lecture Notes in Computational Science and Engineering, Volume 39, Springer, 2004, pp.3-22.
- [18] E.G. Flekkoy, G. Wagner and J. Feder, *Hybrid model for combined particle and continuum dynamics*, Europhys. Lett., 52 (2000), pp.271-276.
- [19] N.G. Hadjiconstantinou, *Hybrid atomistic-continuum formulations and the moving contact-line problem*, J. Comput. Phys., 154 (1999), pp.245-265.
- [20] N.G. Hadjiconstantinou and A.T. Patera, *Heterogeneous atomistic-continuum representation for dense fluid systems*, Intl. J. Modern Phys. C, 8 (1997), pp.967-976.
- [21] J.W. Jerome, *Analysis of Charge Transport, a Mathematical Study of Semiconductor Devices*, Springer, Berlin, 1996.
- [22] G. Jiang and C.-W. Shu, *Efficient implementation of weighted ENO schemes*, J. Comput. Phys., 126 (1996), pp.202-228.
- [23] H. Kadowaki and W.K. Liu, *Bridging multiscale method for localization problems*, Comput. Methods Appl. Mech. Eng., 193 (2004), pp.3267-3302.
- [24] P. Le Tallec and J.P. Perlat, *Coupling kinetic models with Navier-Stokes equations*, CFD Review, 2 (1998), pp.833-855.
- [25] Y. Liu and C.-W. Shu, *Local discontinuous Galerkin methods for moment models in device simulations: formulation and one dimensional results*, J. Comput. Electronics, to appear.
- [26] X. Nie, S. Chen, W. E and M.O. Robbins, *A continuum and molecular dynamics hybrid method for micro- and nano-fluid flow*, J. Fluid Mech., 500 (2004), pp.55-64.

- [27] S.T. O'Connell and P.A. Thompson, *Molecular dynamics-continuum hybrid computations: a tool for studying complex fluid flows*, Phys. Rev. E, 52 (1995), pp.R5792-R5795.
- [28] H.S. Park, E.G. Karpov, W.K. Liu and P.A. Klein, *The bridging scale for two-dimensional atomistic/continuum coupling*, Phil. Mag. A., 85 (2005), pp.79-113.
- [29] D. Qian, G.J. Wagner and W.K. Liu, *A multiscale projection method for the analysis of carbon nanotubes*, Comput. Methods Appl. Mech. Eng., 193 (2004), pp.1603-1632.
- [30] J. Smoller, *Shock Waves and Reaction-Diffusion Equations*, Springer-Verlag, New York, Heidelberg and Berlin, 1983.
- [31] C.-W. Shu and S. Osher, *Efficient implementation of essentially non-oscillatory shock-capturing schemes*, J. Comput. Phys., 77 (1988), pp.439-471.
- [32] K. Xu, *Gas-Kinetic Schemes for Unsteady Compressible Flow Simulations*, von Karman Institute for Fluid Dynamics Lecture Series, 1998-03 (1998).
- [33] J. Yan and C.-W. Shu, *A local discontinuous Galerkin method for KdV type equations*, SIAM J. Numer. Anal., 40 (2002), pp.769-791.